MATERIALS ENGINEERING

Efficient solar-driven water splitting by nanocone $BiVO_4$-perovskite tandem cells

10.1126/sciadv.1501764

Yongcai Qiu,[1,2]* Wei Liu,[2]* Wei Chen,[2]* Wei Chen,[3]* Guangmin Zhou,[2] Po-Chun Hsu,[2] Rufan Zhang,[2] Zheng Liang,[2] Shoushan Fan,[1] Yuegang Zhang,[1,4†] Yi Cui[2,5†]

Bismuth vanadate ($BiVO_4$) has been widely regarded as a promising photoanode material for photoelectrochemical (PEC) water splitting because of its low cost, its high stability against photocorrosion, and its relatively narrow band gap of 2.4 eV. However, the achieved performance of the $BiVO_4$ photoanode remains unsatisfactory to date because its short carrier diffusion length restricts the total thickness of the $BiVO_4$ film required for sufficient light absorption. We addressed the issue by deposition of nanoporous Mo-doped $BiVO_4$ (Mo:$BiVO_4$) on an engineered cone-shaped nanostructure, in which the Mo:$BiVO_4$ layer with a larger effective thickness maintains highly efficient charge separation and high light absorption capability, which can be further enhanced by multiple light scattering in the nanocone structure. As a result, the nanocone/Mo:$BiVO_4$/Fe(Ni)OOH photoanode exhibits a high water-splitting photocurrent of 5.82 ± 0.36 mA cm^{-2} at 1.23 V versus the reversible hydrogen electrode under 1-sun illumination. We also demonstrate that the PEC cell in tandem with a single perovskite solar cell exhibits unassisted water splitting with a solar-to-hydrogen conversion efficiency of up to 6.2%.

INTRODUCTION

Hydrogen (H_2) is a clean and renewable fuel that could be produced by a photoelectrochemical (PEC) water-splitting cell in which semiconductors convert water directly to hydrogen from sunlight (*1*–*4*). Over the past few decades, extensive efforts have been invested to explore oxide-based photoanodes for use in PEC cells because of their relatively good stability in resisting oxidative photocorrosion and their low-cost fabrication (*5*–*12*). Bismuth vanadate ($BiVO_4$) is one of the most important photoanode materials because of its relatively narrow band gap of 2.4 eV and its adequate conduction band edge position relative to the H_2O/H_2 evolution level (*13*–*16*). However, the demonstrated solar-to-hydrogen (STH) conversion efficiency of the material to date is low (<2%), which is largely hindered by its short carrier diffusion length. Generally, the effective thickness of a photoelectrode film is determined by the carrier transport lifetime. To compensate for the short carrier diffusion length, the reported thickness of the $BiVO_4$-based photoanode is usually less than 200 nm. The thin $BiVO_4$ films usually present high transparency, resulting in the transmittance of a large portion of visible light. The ability to use engineered architectures to deposit a thick layer of photoactive materials is essential for high-performance PEC water-splitting and other photovoltaic systems (*17*–*21*). The nanocone structures have been considered as one of the highly promising candidates for high-efficiency thin-film photovoltaics (*22*). However, few studies have explored nanocone-based PEC devices, particularly with porous photoactive layers on nanocone structures. In PEC cells, the photoactive layers deposited on the nanocone conductive substrates may not only enhance the light absorption of the photoactive material but may also maintain efficient charge separation and provide a large contact surface area at the electrode/electrolyte interface to promote the surface water oxidation process. We report here a facile strategy for the deposition of an approximately 700-nm-thick nanoporous Mo-doped $BiVO_4$ (Mo:$BiVO_4$) layer on an engineered cone-shaped nanostructure and demonstrate that the unique photoanode achieves a remarkable water-splitting photocurrent at low applied voltage with the best-reported STH conversion efficiency to date. Our study presents the first successful case for realizing a thick nanoporous photoabsorption layer with highly efficient charge separation through the engineered cone-shaped nanostructure and solves the urgent issue concerning the incompatibility of light absorption capability with carrier transport length. The strategy of depositing photoactive materials on the engineered light-trapping architectures offers a new photoelectrode architecture for high-performance PEC water-splitting cells.

RESULTS

The thickness of the $BiVO_4$ photoelectrode film for water splitting is generally limited by the hole diffusion length of around 100 nm and the film's poor electron transport properties (*23*). The thin photoelectrode film results in insufficient light absorption. Our strategy for depositing a nanoporous $BiVO_4$ on a conductive nanocone substrate is an effective approach to increasing the thickness of the $BiVO_4$ photoelectrode film. The light absorption capability in this unique structure is significantly enhanced not only by the relatively thick nanoporous $BiVO_4$ film but also by the multiple light scattering in the nanocone structure. In addition, the conductive nanocone substrate can achieve efficient charge collection for the relatively thick film (Fig. 1).

The fabrication of the nanoporous Mo:$BiVO_4$ on top of light-trapping nanocone architectures for PEC water-splitting cells is a two-step process. Figure 2A shows the fabrication process of the conductive nanocone architecture (see Materials and Methods) (*24*). The first step is the fabrication of the conductive nanocone substrate.

[1]Department of Physics, Tsinghua University, Beijing 100084, China. [2]Department of Materials Science and Engineering, Stanford University, Stanford, CA 94305, USA. [3]Michael Grätzel Centre for Mesoscopic Solar Cells, Wuhan National Laboratory for Optoelectronics, Huazhong University of Science and Technology, Wuhan 430074, China. [4]Suzhou Institute of Nano-Tech and Nano-Bionics, Chinese Academy of Sciences, Suzhou, Jiangsu 215123, China. [5]SLAC National Accelerator Laboratory, Stanford Institute for Materials and Energy Sciences, 2575 Sand Hill Road, Menlo Park, CA 94025, USA.
*These authors contributed equally to this work.
†Corresponding author. Email: ygzhang2012@sinano.ac.cn (Y.Z.); yicui@stanford.edu (Y.C.)

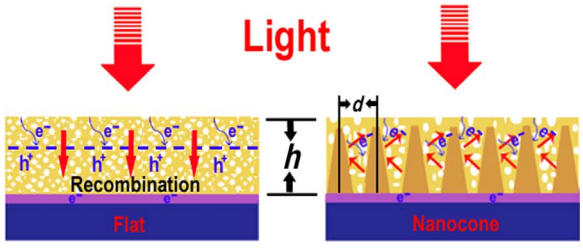

Fig. 1. Schematic illustration of the optical absorption mechanism and electron transport of nanoporous $BiVO_4$ on the flat substrate and the conductive nanocone substrate. The total thickness (*h*) of the $BiVO_4$ film is limited by its short carrier lifetime and poor electron transport properties. A large proportion of photoexcited electrons recombine in the flat photoelectrode film before reaching the electrode. However, the *h* of the $BiVO_4$ film can be increased by introducing the nanocone arrays as a result of the shortened charge transport path that enables efficient charge collection around the conductive nanocones. In addition, its light absorption capability can be further enhanced by multiple light scattering in the unique structure. The half-pitch *d*/2 (~150 to 200 nm) is an optimized carrier diffusion length for our nanoporous Mo:$BiVO_4$.

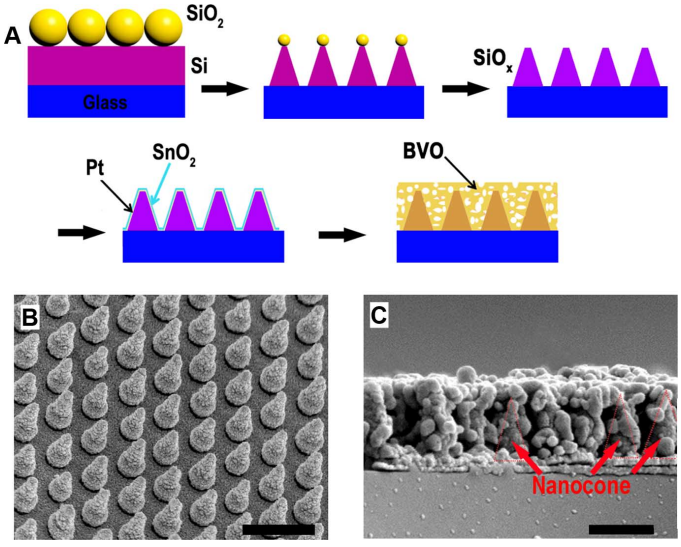

Fig. 2. Schematic illustration of the fabrication process of the conductive nanocone substrate and electron microscope images of Mo:$BiVO_4$ on the nanocone substrate. (**A**) First, the glass/Si substrate was deposited with one close-packed monolayer of SiO_2 to produce a mask for etching and then the shrinking stage was used to adjust the diameter and spacing of the SiO_2 nanoparticles through a selective and isotropic RIE process. Second, a Si nanocone array structure was generated via Cl_2-based RIE of the Si substrate. The subsequent third process is to oxidize Si nanocone arrays at high temperature in air. The fourth step is to prepare conductive nanocone substrates by coating one layer of Pt and another functional layer of SnO_2. The final step is to deposit the nanoporous $BiVO_4$ photoactive layer through a sol-gel process. (**B**) Scanning electron microscope (SEM) images (60° tilting) of the final SiO_x/Pt/SnO_2 nanocone arrays. (**C**) Cross-sectional SEM images of Mo:$BiVO_4$ on the SiO_x/Pt/SnO_2 nanocone substrate. Some exposed nanocones were also marked in the figure. Scale bars, 500 nm.

The approximately 1000-nm-thick amorphous Si was deposited on quartz- or F-doped SnO_2 (FTO)–coated glass substrates using the AJA sputtering system. Then, SiO_2 nanoparticles with a diameter of 500 nm were assembled to form a close-packed monolayer on top of the glass/Si thin film using the Langmuir-Blodgett (LB) method. The diameter and spacing of the SiO_2 nanoparticles can be adjusted to form a mask for the Cl_2-based reactive ion etching (RIE) process. Si nanocone arrays were formed after the RIE process (fig. S1). The SEM images show that each nanocone has a height of ~600 nm. The base and tip diameters of these nanocones are approximately 300 and 50 nm, respectively. Magnetron sputtering of Pt, followed by the coating of thin SnO_2 using the ultrasonic spray pyrolysis (USP) method, was used to create conductive nanocone arrays on the glass substrate (Fig. 2B and fig. S2). The thin SnO_2 layer plays an important role in forming a staggered band gap alignment feature with Mo:$BiVO_4$ (fig. S3). In general, the band alignment feature in semiconductors facilitates efficient electron-hole separation for light harvesting.

The second step is the synthesis of nanoporous Mo:$BiVO_4$. The nanoporous Mo:$BiVO_4$ layer was prepared by a facile sol-gel process (see Materials and Methods and fig. S4). To obtain high-performance Mo:$BiVO_4$ films, we prepared the $BiVO_4$ films with different Mo-doping concentrations on FTO-coated glass. NH_4MoO_4 served as the Mo source to substitute the V atoms in $BiVO_4$, which can effectively enhance the charge separation. Powder x-ray diffraction (XRD) revealed that the resulting film has a pure monoclinic scheelite phase, with no secondary phases (fig. S5). The Mo:$BiVO_4$ photoelectrodes with the highest photocurrent (fig. S6) show that the Mo element is indeed doped into $BiVO_4$, as evidenced by x-ray photoelectron spectroscopy (XPS) (fig. S7). The result is consistent with other optimum doping concentrations (~3%) for Mo:$BiVO_4$ (*23*). The SEM images (fig. S4) reveal that the grains with a diameter of approximately 100 nm or less were interconnected. The feature facilitates efficient charge transport in the nanoporous photoelectrode. The optimized Mo:$BiVO_4$ film was then deposited on our designed conductive nanocone substrates (Fig. 2C). For comparison, the Mo:$BiVO_4$ on conductive flat substrates with the same thickness was also prepared (fig. S4).

To confirm the light trapping of the nanocone structures, we first investigated their optical properties after nanoporous Mo:$BiVO_4$ deposition. The ultraviolet-visible (UV-VIS) absorption spectra (Fig. 3A) show that the light absorption on the nanocone substrate is much stronger than that on the FTO-coated glass, indicating strong light trapping in the nanocone substrate. The band gap of the nanoporous Mo:$BiVO_4$ is approximately 2.4 eV (fig. S8), which is similar to previous reports (*15*, *25*, *26*). The experimental results are in agreement with those obtained from finite-difference time-domain simulations (Fig. 3B).

To further shed light on how light is coupled into the nanocone structure, we plotted the cross-sectional electric field intensity ($|E|$) distribution of the electromagnetic (EM) wave at 500 nm (Fig. 3B). Because the distance between neighboring nanocone arrays is close to the incident light wavelength, the incident light becomes diffracted and the EM wave redistributes in the nanocone area, resulting in a significant enhancement of EM field around the nanocone structure. The yellow and red hot area in the porous Mo:$BiVO_4$ representing strong light absorption on the nanocone substrate is much greater than that on the flat substrate, indicating the significant light-trapping enhancement by using the nanocone photoelectrode. Additionally, the cross-sectional $|E|$ distribution of the nanocone structure demonstrates a lower reflection than that of the FTO-coated glass, denoted by the darker color above the

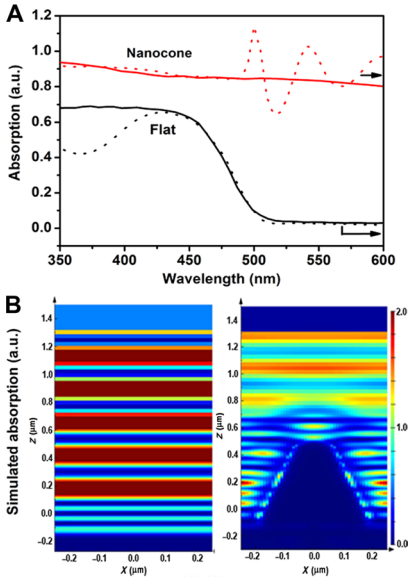

Fig. 3. Optical absorption measurement and simulation. (**A**) UV-VIS optical absorption (solid line) of Mo:$BiVO_4$ on the nanocone substrate and the FTO-coated glass and their corresponding simulated air mass (AM) 1.5-G spectrum–integrated absorption (dashed line). (**B**) Comparison of simulated cross-sectional |*E*| distribution of the EM wave at 500 nm in Mo:$BiVO_4$ on the nanocone substrate and the FTO-coated glass. The red hot area, which represents high generation, indicates effective light trapping by nanocone arrays. A 200-nm-thick $BiVO_4$ on FTO-coated glass and a 700-nm-thick $BiVO_4$ on the SnO_2/Pt (50 nm/80 nm) nanocone substrate were used to perform the simulations, respectively. a.u., arbitrary units.

light source above Z = 1.3 μm, indicating that more light has been trapped in the nanocone structure. The EM field around the Mo:$BiVO_4$ has been significantly enhanced, leading to more efficient absorption by the photoactive material.

The excellent light absorption capability of the nanocone structures is essential for high-performance PEC water-splitting cells. Figure 4A shows the typical photocurrent-potential (*J-V*) curves [*V* is with respect to the reversible hydrogen electrode (RHE); *E*(RHE) = *E*(Ag/AgCl) + 0.1976 V + 0.059 pH] of Mo:$BiVO_4$ films on the nanocone substrate and the FTO-coated glass substrate. Upon sweeping the potential from 0.2 to 1.5 V versus RHE under 1-sun illumination (100 mW cm^{-2}), it can be clearly seen that the Mo:$BiVO_4$ deposited on the nanocone substrate showed a photocurrent density of 4.18 ± 0.25 mA cm^{-2} at 1.23 V versus RHE, which is almost two times higher than that on the flat one (2.10 ± 0.14 mA cm^{-2}). The photocurrent is among the highest achieved with $BiVO_4$ without using a hole scavenger and an oxygen evolution reaction (OER) catalyst (*26*–*29*). The highest applied bias photon-to-current efficiency (ABPE) of ~0.74% was reached at a high voltage of 0.87 V versus RHE (fig. S9). The high voltage is a sign of low fill factor and high photocurrent onset potential due to the intrinsic poor catalytic activity of $BiVO_4$ for water oxidation. The issue can be addressed by incorporating an OER catalyst into $BiVO_4$.

Before the deposition of the catalyst, the optimized nanocone/Mo:$BiVO_4$ photoanode was first investigated in the same phosphate buffer solution containing 0.5 M sodium sulfite (Na_2SO_3) as the hole scavenger. Figure 4B shows its *J-V* curve for sulfite oxidation. The oxidation of sulfite is thermodynamically and kinetically more favorable than water oxidation (*30*). The photocurrent for sulfite oxidation is independent from that for PEC water splitting as a result of the poor water oxidation kinetics of $BiVO_4$. The results show that a photocurrent density of 3.45 ± 0.30 mA cm^{-2} was achieved at a potential of as low as 0.54 V versus RHE, and 6.05 ± 0.30 mA cm^{-2} (80.7% of the theoretical value of $BiVO_4$ with a 2.4-eV band gap) was achieved at a potential of 1.23 V versus RHE.

As reported previously, the photocurrent onset potential of $BiVO_4$ for oxygen evolution can be cathodically shifted by 0.1 to 0.3 V with an OER catalyst (for example, FeOOH, FeOOH/NiOOH, and Co-Pi) (*14*, *27*, *29*). Meanwhile, the OER catalysts play an important role in the rapid increase in photocurrent at relatively low potential, which represents an improved fill factor. They have also been proven to effectively suppress photocorrosion under illumination, resulting in an improved stability of photoanodes. Therefore, an active OER catalyst of Fe(Ni)OOH was prepared on a nanoporous Mo:$BiVO_4$-absorbed layer using a facile two-step electrochemical deposition technique (see Materials and Methods). The transmission electron microscope (TEM) image in fig. S10 clearly shows that the Fe(Ni)OOH layer was homogeneously deposited on the surface of Mo:$BiVO_4$ particles. Energy-dispersive x-ray (EDX) spectrum further confirms the successful coating of the Fe(Ni)OOH layer on Mo:$BiVO_4$ particles (fig. S10).

Figure 4B shows a significant photocurrent improvement for water oxidation achieved with the coating of the Fe(Ni)OOH layer. The optimized nanocone/Mo:$BiVO_4$/Fe(Ni)OOH photoanode reached a photocurrent density of 5.82 ± 0.36 mA cm^{-2} at 1.23 V versus RHE, which approaches ~77.8% of the theoretical value. A cathodic shift of the photocurrent onset potential by ~0.10 V and a rapid photocurrent increase from 0.3 to 0.6 V versus RHE resulted in the highest ABPE of ~2.05% at 0.62 V versus RHE (fig. S8). The performance is slightly lower than expected from sulfite oxidation (Fig. 4, B and C) but is almost the best reported for $BiVO_4$-based PEC cells to date (*14*, *29*). The result is further demonstrated using incident photon-to-electron conversion efficiency (IPCE) measurements (Fig. 4C). The nanocone/Mo:$BiVO_4$/Fe(Ni)OOH photoanode for water oxidation shows that the IPCE value is more than 75% below 460 nm, which is slightly lower than the value of the nanocone/Mo:$BiVO_4$ photoanode for sulfite oxidation (>82% below 460 nm), in accordance with the *J-V* measurements. In addition, the optimized nanocone/Mo:$BiVO_4$/Fe(Ni)OOH photoanode is stable under water oxidation conditions, which is demonstrated through a 5-hour stability test (fig. S11).

To further understand the charge transport effect of the nanocone structure on PEC performance enhancement, measurements of Mo:$BiVO_4$ on the conductive flat substrate and on the nanocone substrate with the same film thickness of ~700 nm (see Fig. 2 and fig. S4) were performed in a 0.5 M phosphate (pH 7) buffer solution containing 0.5 M Na_2SO_3. The thick Mo:$BiVO_4$ on the flat substrate only delivered a photocurrent density of 2.93 ± 0.12 mA cm^{-2} at 1.23 V versus RHE, which is much smaller than that on the nanocone substrate (6.05 ± 0.30 mA cm^{-2}) (fig. S12), suggesting that a large proportion of photogenerated carriers recombine in the flat photoelectrode film before reaching the electrode. In other words, charge transport in the nanocone structure remains efficient despite the thick Mo:$BiVO_4$ layer as a result of the shortened carrier diffusion length induced by the conductive nanocone arrays (Fig. 1).

The remarkable angular-independent light-scattering capability is another important feature for the nanocone structure. Nanocone structures have shown a promising light-trapping capability over a

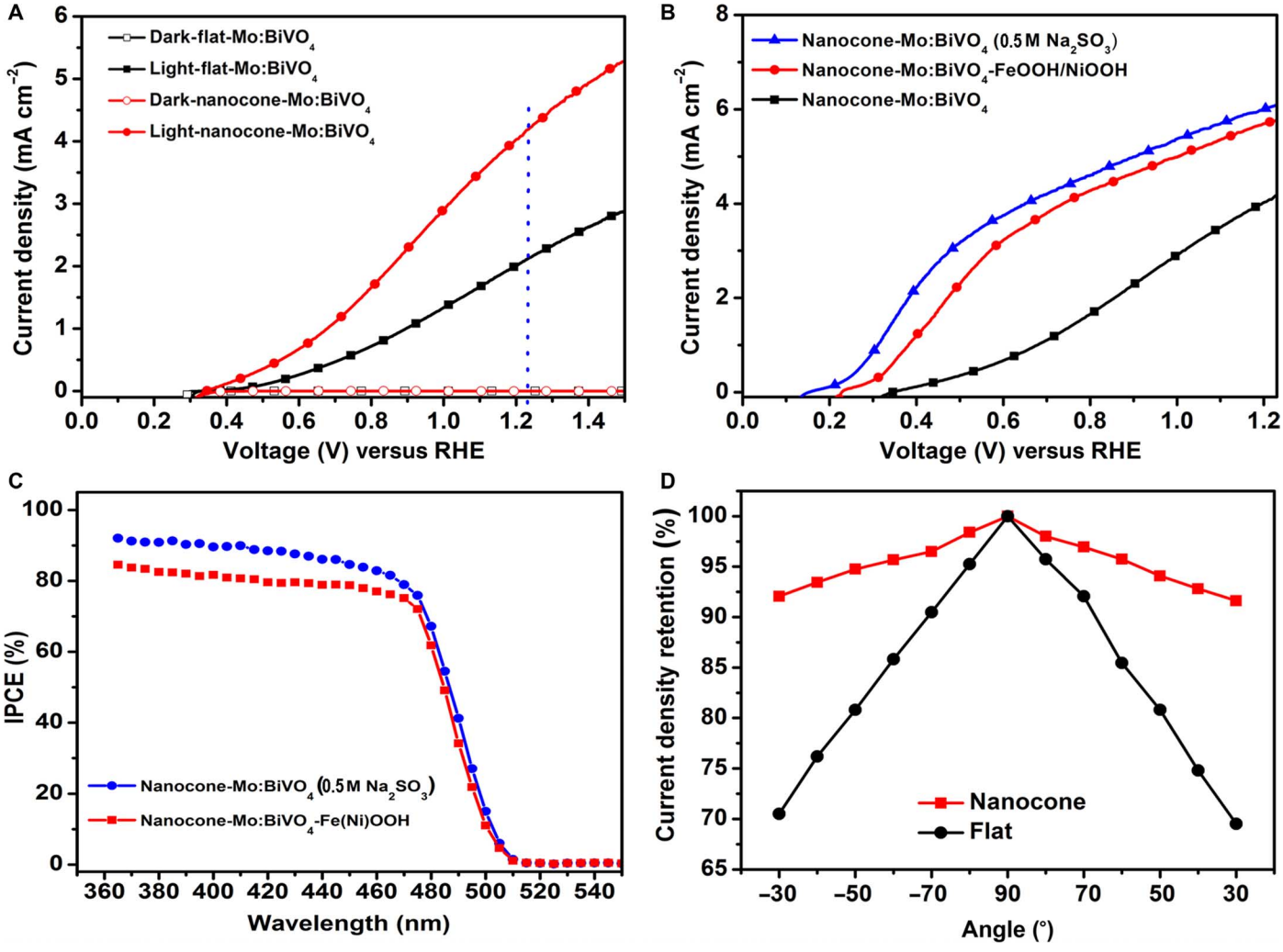

Fig. 4. PEC test. (**A**) *J-V* curves of the Mo:$BiVO_4$ on the FTO-coated glass and the nanocone substrate tested in a 0.5 M KH_2PO_4 buffer solution (pH 7) and at a scan rate of 20 mV s^{-1}. The corresponding dark currents are also shown. (**B**) *J-V* curves of the nanocone/Mo:$BiVO_4$ film measured in phosphate buffer solution containing 0.5 M Na_2SO_3 and the nanocone/Mo:$BiVO_4$/Fe(Ni)OOH film measured in phosphate buffer solution. The *J-V* curve of the nanocone/Mo:$BiVO_4$ is also shown. (**C**) IPCE spectra of the nanocone/Mo:$BiVO_4$ film tested in 0.5 M Na_2SO_3 and the nanocone/Mo:$BiVO_4$/Fe(Ni)OOH film tested in phosphate buffer solution with bias at 1.23 V versus RHE. (**D**) Comparison of the angular independence of photocurrent between the flat substrate and the nanocone substrate, showing only a slight decrease in photocurrent for the latter going from 0° to 60° irradiation.

broad range of wavelengths and incident angles (*19*, *20*, *31*–*33*). Figure 4D shows the achieved photocurrent at 1.23 V versus RHE as a function of incident light. Compared to the 29.4% loss for Mo:$BiVO_4$ on the flat substrate, the photocurrent density for the nanocone substrate only dropped by 8.1% with the largest irradiation angle (60°). The results demonstrate that the nanocone structure has an omnidirectional light-harvesting capability, which is highly favorable for practical applications.

The ABPE of the nanocone/Mo:$BiVO_4$/Fe(Ni)OOH photoanode was calculated using a chopped *J-V* curve obtained in a two-electrode configuration (fig. S13). The maximum ABPE of ~1.92% was achieved with a water-splitting photocurrent of ~3.21 mA cm^{-2} at a low applied voltage of 0.63 V, which is close to that obtained in a three-electrode configuration (~2.05%). We also evaluated reproducibility by testing batches of the photoanodes, and their ABPE distribution is shown in fig. S14. The ABPE ranges between 1.75 and 1.92%, indicating the reproducibility of our designed photoanodes. The photoanode with high efficiency at low applied voltage is certainly highly preferable for achieving self-biased operation in tandem with other photovoltaics.

A perovskite solar cell (PSC) is a promising candidate for tandem devices because of its high potential and high efficiency. The PSC was prepared following our previous work (*34*). The PSC could deliver a stable power conversion efficiency of ~15.5% under 1-sun irradiation (fig. S15). To construct a PSC-PEC tandem device, we used a beam splitter to separate a standard solar cell (1 sun) into two light beams (see Materials and Methods and Fig. 5A). Figure 5B shows separately measured *J-V* curves of the PSC and the PEC cells with intersection

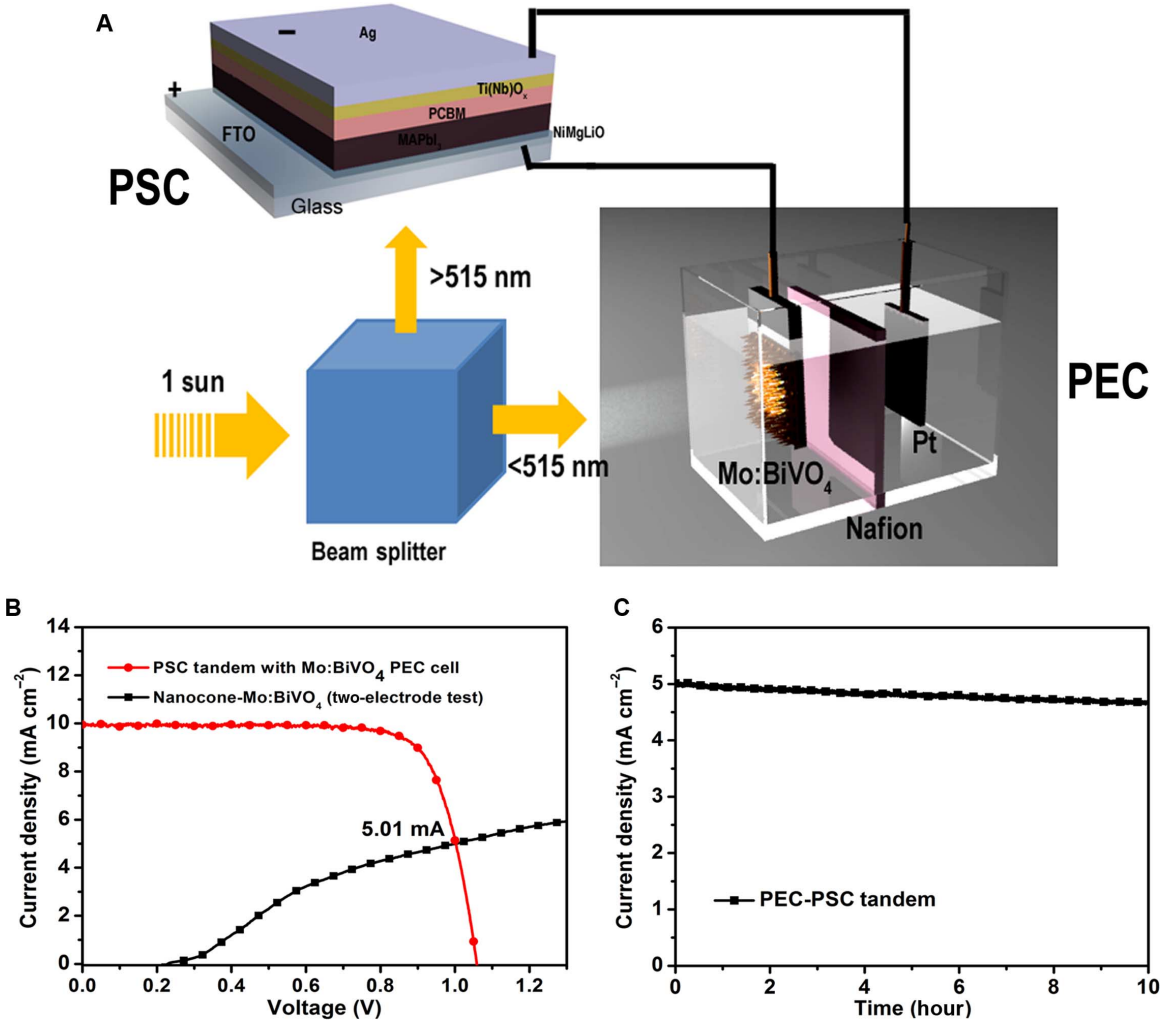

Fig. 5. PEC-PSC tandem device. (**A**) The configuration of the PEC-PSC tandem device. (**B**) *J-V* curves of the PSC (>515 nm) and the nanocone/Mo:$BiVO_4$ photoanode (<515 nm) measured at 1 sun. (**C**) J_{OP} versus time profiles measured for the PEC-PSC tandem over 10 hours.

points at 5.01 mA. The photocurrent corresponds to the theoretical STH efficiency of 6.2%. A similar tandem design based on a PEC cell made of Fe_2O_3 and a PSC has been reported with an efficiency of only 2.4% (*35*). The performance of our device is more than two times higher because a more efficient PEC cell based on Mo-doped $BiVO_4$ nanocones was used. Although some studies have reported using solar cells to split water with more than 10% efficiency (*36*–*38*), such devices are based on solar cells connecting with nonphotoactive catalytic electrodes. In principle, they are single-junction devices. According to the well-known Shockley-Queisser limitation, their theoretical maximum solar conversion efficiency is ~34%. In contrast, our design is a double-junction device that is made up of a combination of a photoactive PEC cell and a PSC. Double-junctions device have a higher theoretical maximum efficiency of more than 45%. Although the efficiency we have demonstrated in this work is only 6.2%, our device has much room for further improvement in the future.

A stability test of the tandem device was performed over 10 hours (Fig. 5C). It showed only 5.8% decay, indicating decent stability for water oxidation of our PEC-PSC tandem cell. The stability also further demonstrates the stable PSC with inorganic charge extraction layers (*34*). After 10 hours of PEC test, the morphology of the Mo:$BiVO_4$/Fe(Ni)OOH does not change significantly (fig. S16), which is ascribed to the protection of the Fe(Ni)OOH layer against the photocorrosion of Mo:$BiVO_4$ (*23*). H_2 and O_2 production was detected with gas chromatography (GC) (fig. S17). The molar ratio of the produced H_2/O_2 was close to 2:1. The amount of generated H_2 is ~85.5 μmol cm^{-2} hour^{-1}, corresponding to a photocurrent-to-H_2 Coulombic efficiency of ~92% for the tandem device. The slight deviation is likely due to our imperfect manual sampling method of H_2 for GC analysis.

DISCUSSION

In summary, we have reported a facile approach for the deposition of a nanoporous Mo:$BiVO_4$ layer on an engineered cone-shaped nanophotonic structure. After deposition of Fe(Ni)OOH, the photoanode can

deliver a remarkable photocurrent density of 5.82 ± 0.36 mA cm^{-2} at 1.23 V versus RHE. The photoanode in tandem with a single PSC produced a photocurrent of 5.01 mA cm^{-2}, corresponding to the theoretical STH efficiency of 6.2%. Our study presents the first successful case for realizing a nanoporous photoabsorption layer with highly efficient charge transport through depositing the material on the engineered cone-shaped nanostructure. The significant advance demonstrated here indicates that the deposition of photoactive materials on an engineered light-trapping architecture offers a new avenue for efficient PEC water splitting as well as for high-efficiency photovoltaic cells.

MATERIALS AND METHODS

Preparation of the conductive nanocone substrate

Si nanocone arrays on quartz- or FTO-coated glass substrates were first fabricated on the basis of our previous report (*24*, *31*). A 1-μm-thick amorphous Si film was grown using the AJA sputtering system on quartz- or FTO-coated glass substrates. SiO_2 nanoparticles with a diameter of 500 nm were then assembled using the LB method, giving rise to one close-packed monolayer on top of the Si thin film. Monodisperse SiO_2 nanoparticles with a diameter of 500 nm were produced by a modified Stober synthesis (*31*). Before the LB deposition of the monolayer, these nanoparticles were modified with aminopropyl methyldiethoxysilane so that they could be terminated with positively charged amine groups to prevent aggregation. The diameter and spacing of the nanospheres were tuned by selective and isotropic RIE on the basis of fluorine chemistry using CHF_3. These shrunk silica nanoparticles were then used as an etch mask during a Cl_2-based RIE process to fabricate nanocones in one step. The formed Si nanocone arrays were oxidized at 650°C for 10 hours to generate SiO_2 nanocone arrays. An 80-nm-thick Pt layer and an approximately 50-nm-thick SnO_2 layer were subsequently coated on SiO_2 nanocone arrays, respectively, through magnetron sputtering and the USP method. More details can be found in our previous work (*20*, *21*).

Preparation of nanoporous Mo-doped $BiVO_4$ on the conductive nanocone substrate

A precursor solution for the preparation of $BiVO_4$ photoelectrodes contains 0.5 M bismuth nitrate and 0.6 M vanadyl isopropoxide in acetylacetonate and ethanol [50:50 (v/v)]. The precursor solution was deposited on the nanocone substrates or the FTO-coated glass substrates using a controllable spin-coating technique. $BiVO_4$ photoelectrodes were obtained by annealing the samples at 300°C for 1 hour and at 450°C for 2 hours with a ramping rate of 2°C/min. Excess V_2O_5 was removed in 1 M NaOH solution at 50°C for 15 min with gentle stirring. The resulting $BiVO_4$ photoelectrodes were rinsed with water for several times to remove the residue solution and then air-dried at room temperature. A certain amount of $(NH_4)MoO_4$ dissolved in acetylacetonate and acetic acid, which served as doping sources, was added in the above precursor solution. The highest photocurrent of Mo:$BiVO_4$ photoelectrodes was obtained with a Mo-doping concentration of ~3%.

Electrodeposition of $Fe(OH)_2$/$Ni(OH)_2$. The $Fe(OH)_2$/$Ni(OH)_2$ nanoparticles were prepared by a facile two-step electrochemical deposition technique. The deposition was conducted in a three-electrode setup, with nanoporous Mo:$BiVO_4$ as the working electrode, saturated calomel electrode (Accumet, Fisher Scientific) as the reference electrode, and platinum wire as the counter electrode in a freshly prepared solution of 50 mM $(NH_4)_2Fe(SO_4)_2$ and 50 mM $Ni(NO_3)_2$. The electrodeposition of $Fe(OH)_2$/$Ni(OH)_2$ was first applied at −0.5 V in a 50 mM $(NH_4)_2Fe(SO_4)_2$ aqueous solution for 2 min and was then applied at −0.45 V in a 50 mM $Ni(NO_3)_2$ aqueous solution for another 2 min. After electrodeposition, the electrode was rinsed with water several times to remove the residue solution and then air-dried at room temperature. When irradiated by sunlight, the photogenerated holes from Mo:$BiVO_4$ converts $Fe(OH)_2$/$Ni(OH)_2$ into FeOOH/NiOOH [Fe(Ni)OOH], which will promote the OER.

Optical measurements

Standard hemispherical measurements were carried out with an integrating sphere (Newport). More details can be found in our previous paper (*31*). FTO glass was used as the reference for these absorption measurements. To construct a PEC-PSC tandem, a standard solar light (1 sun) was separated into two beams by a beam splitter (515 nm). The light beam (<515 nm) was used for testing the performance of PEC cells, and the other light beam was used for measuring the performance of PSCs.

PEC measurements. Mo:$BiVO_4$ photoelectrodes were used as the working electrode, a Pt net served as the counter electrode, and an Ag/AgCl was used as the reference electrode. All electrodes were immersed in a quartz electrolytic cell; the photoelectrode was covered by ethoxyline except for a window for light illumination. All illuminated areas were 0.25 cm^2. The simulated solar illumination was obtained by passing light from a 300-W Xe arc lamp through a water filter (infrared filter), neutral density filters, or an AM 1.5-G filter. The power density of the incident light was calibrated to 100 mW/cm^2 by using a thermopile detector and a National Renewable Energy Laboratory–certified reference cell. Photocurrent measurements were performed in a 0.5 M potassium phosphate (KH_2PO_4) buffer solution (pH 7) with or without 0.5 M Na_2SO_3 as a hole scavenger [reported with respect to the RHE; $E(\mathrm{RHE}) = E(\mathrm{Ag/AgCl}) + 0.1976\ \mathrm{V} + 0.059\ \mathrm{pH}$]. Ar gas was purged through the cell during the measurement to instantaneously flush away O_2 from the working electrode. *J-V* curves were measured by sweeping the potential to the positive direction with a scan rate of 20 mV s^{-1}. *J-V* curves were also obtained with chopped illumination to examine transient photocurrents. IPCE spectra were measured using the Zahner ZENNIUM CIMPS system. IPCE was measured at the reversible water oxidation potential of 1.23 V versus RHE in 0.5 M phosphate buffer (pH 7) using the same three-electrode setup described above for photocurrent measurements.

The efficiency (η) for a water-splitting photoelectrode that requires an applied bias can be evaluated using the equation

$$\eta = I(1.23 - V_{\mathrm{app}})/P_{\mathrm{light}}$$

where V_{app} is the applied voltage versus RHE, I is the externally measured current density, and P_{light} is the power density of the illumination.

The overall water-splitting efficiency (η_{STH}) of the photoelectrolysis system is estimated by overlapping the individual *J-V* curve obtained for a PSC and a photoanode and can be calculated using

$$\eta_{\mathrm{STH}} = 1.23(J_{\mathrm{OP}})/P_{\mathrm{light}}$$

where J_{OP} is the maximum operating current density for the integrated PEC system, which is the current density at the intersection of the two *J-V* curves.

H_2 and O_2 measurements were carried out in the airtight cell using GC to analyze the headspace. The amounts of H_2 and O_2 gas evolved were determined by taking 1 ml of gas from the headspace of the cell using a syringe and injecting it into the gas-sampling loop of the GC every hour.

SUPPLEMENTARY MATERIALS

Supplementary material for this article is available at http://advances.sciencemag.org/cgi/content/full/2/6/e1501764/DC1

fig. S1. SEM images of the Si nanocone arrays with the tips of SiO_2, Si nanocone arrays, and Mo:$BiVO_4$ on SiO_x/Pt/SnO_2 nanocone arrays.

fig. S2. SEM images with different magnifications of the conductive nanocone substrate.

fig. S3. Band energy diagram of the designed $BiVO_4$-based photoanode.

fig. S4. SEM images of nanoporous Mo:$BiVO_4$ on the Pt-coated glass and the FTO-coated glass substrates.

fig. S5. XRD pattern of nanoporous Mo:$BiVO_4$.

fig. S6. PEC water-splitting performance of $BiVO_4$ on the FTO-coated glass with different Mo-doping concentrations tested in pH 7 phosphate buffer solution.

fig. S7. High-resolution Bi, V, and Mo XPS spectra of 3% Mo:$BiVO_4$.

fig. S8. Band gap of 3% Mo-doped $BiVO_4$.

fig. S9. The ABPE obtained from *J-V* curves in Fig. 4B according to the equation $\eta = I\ (1.23 - V_{app})/P_{light}$.

fig. S10. A typical TEM image of Fe(Ni)OOH nanoparticles on Mo:$BiVO_4$ and its corresponding EDX spectrum.

fig. S11. Photocurrent density versus time responses of the optimized nanocone/Mo:$BiVO_4$/Fe(Ni)OOH photoanode over 5 hours at 1.23 V versus RHE.

fig. S12. Sulfite oxidation measurements of Mo:$BiVO_4$ on the conductive flat substrate and the nanocone substrate with the same film thickness of ~700 nm (see Fig. 2 and fig. S3) performed in pH 7 phosphate buffer solution containing 0.5 M Na_2SO_3.

fig. S13. *J-V* characteristics of the optimized nanocone Mo:$BiVO_4$/Fe(Ni)OOH photoanode measured using a two-electrode (a working electrode and a Pt counter electrode) method in pH 7 phosphate buffer solution.

fig. S14. The distribution of ABPE by measurements of batches of photoanodes performed in a two-electrode system.

fig. S15. *J-V* curve of a PSC measured under 1-sun irradiation.

fig. S16. The morphology of the Mo:$BiVO_4$/Fe(Ni)OOH after 10 hours of PEC test.

fig. S17. H_2 and O_2 production from the tandem device and the theoretical gas production rate of the tandem device.

REFERENCES AND NOTES

1. M. G. Walter, E. L. Warren, J. R. McKone, S. W. Boettcher, Q. Mi, E. A. Santori, N. S. Lewis, Solar water splitting cells. *Chem. Rev.* **110**, 6446–6473 (2010).
2. K. Ohashi, J. Mccann, J. O. Bockris, Stable photoelectrochemical cells for splitting of water. *Nature* **266**, 610–611 (1977).
3. F. E. Osterloh, Inorganic nanostructures for photoelectrochemical and photocatalytic water splitting. *Chem. Soc. Rev.* **42**, 2294–2320 (2013).
4. C. R. Cox, M. T. Winkler, J. J. H. Pijpers, T. Buonassisi, D. G. Nocera, Interfaces between water splitting catalysts and buried silicon junctions. *Energy Environ. Sci.* **6**, 532–538 (2013).
5. T. Hisatomi, J. Kubota, K. Domen, Recent advances in semiconductors for photocatalytic and photoelectrochemical water splitting. *Chem. Soc. Rev.* **43**, 7520–7535 (2014).
6. Y. Lin, G. Yuan, S. Sheehan, S. Zhou, D. Wang, Hematite-based solar water splitting: Challenges and opportunities. *Energy Environ. Sci.* **4**, 4862–4869 (2011).
7. M. T. Mayer, Y. Lin, G. Yuan, D. Wang, Forming heterojunctions at the nanoscale for improved photoelectrochemical water splitting by semiconductor materials: Case studies on hematite. *Acc. Chem. Res.* **46**, 1558–1566 (2013).
8. G. Wang, X. Lu, Y. Li, Low-cost nanomaterials for photoelectrochemical water splitting, in *Low Cost Nanomaterials* (Springer, London, 2014), pp. 267–295.
9. R. Zhang, D. Shen, M. Xu, D. Feng, W. Li, G. Zheng, R. Che, A. A. Elzatahry, D. Zhao, Ordered macro-/mesoporous anatase films with high thermal stability and crystallinity for photoelectrocatalytic water-splitting. *Adv. Energy Mater.* **4**, 1301725 (2014).
10. W. Li, P. Da, Y. Zhang, Y. Wang, X. Lin, X. Gong, G. Zheng, WO_3 nanoflakes for enhanced photoelectrochemical conversion. *ACS Nano* **8**, 11770–11777 (2014).
11. C. Liu, J. Tang, H. M. Chen, B. Liu, P. Yang, A fully integrated nanosystem of semiconductor nanowires for direct solar water splitting. *Nano Lett.* **13**, 2989–2992 (2013).
12. B. Liu, C.-H. Wu, J. Miao, P. Yang, All inorganic semiconductor nanowire mesh for direct solar water splitting. *ACS Nano* **8**, 11739–11744 (2014).
13. R. Li, F. Zhang, D. Wang, J. Yang, M. Li, J. Zhu, X. Zhou, H. Han, C. Li, Spatial separation of photogenerated electrons and holes among {010} and {110} crystal facets of $BiVO_4$. *Nat. Commun.* **4**, 1432 (2013).
14. T. W. Kim, K.-S. Choi, Nanoporous $BiVO_4$ photoanodes with dual-layer oxygen evolution catalysts for solar water splitting. *Science* **343**, 990–994 (2014).
15. M. Zhou, J. Bao, Y. Xu, J. Zhang, J. Xie, M. Guan, C. Wang, L. Wen, Y. Lei, Y. Xie, Photoelectrodes based upon Mo:$BiVO_4$ inverse opals for photoelectrochemical water splitting. *ACS Nano* **8**, 7088–7098 (2014).
16. M. Zhou, H. B. Wu, J. Bao, L. Liang, X. W. Lou, Y. Xie, Ordered macroporous $BiVO_4$ architectures with controllable dual porosity for efficient solar water splitting. *Angew. Chem.* **52**, 8579–8583 (2013).
17. F. Boudoire, R. Toth, J. Heier, A. Braun, E. C. Constable, Photonic light trapping in self-organized all-oxide microspheroids impacts photoelectrochemical water splitting. *Energy Environ. Sci.* **7**, 2680–2688 (2014).
18. K. X. Wang, Z. Yu, V. Liu, A. Raman, Y. Cui, S. Fan, Light trapping in photonic crystals. *Energy Environ. Sci.* **7**, 2725–2738 (2014).
19. K. X. Wang, Z. Yu, V. Liu, Y. Cui, S. Fan, Absorption enhancement in ultrathin crystalline silicon solar cells with antireflection and light-trapping nanocone gratings. *Nano Lett.* **12**, 1616–1619 (2012).
20. J. Li, Y. Qiu, Z. Wei, Q. Lin, Q. Zhang, K. Yan, H. Chen, S. Xiao, Z. Fan, S. Yang, A three-dimensional hexagonal fluorine-doped tin oxide nanocone array: A superior light harvesting electrode for high performance photoelectrochemical water splitting. *Energy Environ. Sci.* **7**, 3651–3658 (2014).
21. Y. Qiu, S.-F. Leung, Q. Zhang, B. Hua, Q. Lin, Z. Wei, K.-H. Tsui, Y. Zhang, S. Yang, Z. Fan, Efficient photoelectrochemical water splitting with ultrathin films of hematite on three-dimensional nanophotonic structures. *Nano Lett.* **14**, 2123–2129 (2014).
22. M. L. Brongersma, Y. Cui, S. Fan, Light management for photovoltaics using high-index nanostructures. *Nat. Mater.* **13**, 451–460 (2014).
23. L. Chen, F. M. Toma, J. K. Cooper, A. Lyon, Y. Lin, I. D. Sharp, J. W. Ager, Mo-doped $BiVO_4$ photoanodes synthesized by reactive sputtering. *ChemSusChem.* **8**, 1066–1071 (2015).
24. C.-M. Hsu, S. T. Connor, M. X. Tang, Y. Cui, Wafer-scale silicon nanopillars and nanocones by Langmuir-Blodgett assembly and etching. *Appl. Phys. Lett.* **93**, 133109 (2008).
25. A. J. E. Rettie, H. C. Lee, L. G. Marshall, J.-F. Lin, C. Capan, J. Lindemuth, J. S. McCloy, J. Zhou, A. J. Bard, C. B. Mullins, Combined charge carrier transport and photoelectrochemical characterization of $BiVO_4$ single crystals: Intrinsic behavior of a complex metal oxide. *J. Am. Chem. Soc.* **135**, 11389–11396 (2013).
26. Q. Jia, K. Iwashina, A. Kudo, Facile fabrication of an efficient $BiVO_4$ thin film electrode for water splitting under visible light irradiation. *Proc. Natl. Acad. Sci. U.S.A.* **109**, 11564–11569 (2012).
27. S. K. Pilli, T. E. Furtak, L. D. Brown, T. G. Deutsch, J. A. Turner, A. M. Herring, Cobalt-phosphate (Co-Pi) catalyst modified Mo-doped $BiVO_4$ photoelectrodes for solar water oxidation. *Energy Environ. Sci.* **4**, 5028–5034 (2011).
28. P. M. Rao, L. L. Cai, C. Liu, I. S. Cho, C. H. Lee, J. M. Weisse, P. D. Yang, X. L. Zheng, Simultaneously efficient light absorption and charge separation in WO_3/$BiVO_4$ core/shell nanowire photoanode for photoelectrochemical water oxidation. *Nano Lett.* **14**, 1099–1105 (2014).
29. Y. Pihosh, I. Turkevych, K. Mawatari, J. Uemura, Y. Kazoe, S. Kosar, K. Makita, T. Sugaya, T. Matsui, D. Fujita, M. Tosa, M. Kondo, T. Kitamori, Photocatalytic generation of hydrogen by core-shell WO_3/$BiVO_4$ nanorods with ultimate water splitting efficiency. *Sci. Rep.* **5**, 11141 (2015).
30. J. A. Seabold, K.-S. Choi, Efficient and stable photo-oxidation of water by a bismuth vanadate photoanode coupled with an iron oxyhydroxide oxygen evolution catalyst *J. Am. Chem. Soc.* **134**, 2186–2192 (2012).
31. J. Zhu, Z. Yu, G. F. Burkhard, C.-M. Hsu, S. T. Connor, Y. Xu, Q. Wang, M. McGehee, S. Fan, Y. Cui, Optical absorption enhancement in amorphous silicon nanowire and nanocone arrays. *Nano Lett.* **9**, 279–282 (2009).
32. S. Jeong, M. D. McGehee, Y. Cui, All-back-contact ultra-thin silicon nanocone solar cells with 13.7% power conversion efficiency. *Nat. Commun.* **4**, 2950 (2013).
33. C.-M. Hsu, C. Battaglia, C. Pahud, Z. Ruan, F.-J. Haug, S. Fan, C. Ballif, Y. Cui, High-efficiency amorphous silicon solar cell on a periodic nanocone back reflector. *Adv. Energy Mater.* **2**, 628–633 (2012).
34. W. Chen, Y. Wu, Y. Yue, J. Liu, W. Zhang, X. Yang, H. Chen, E. Bi, I. Ashraful, M. Grätzel, L. Han, Efficient and stable large-area perovskite solar cells with inorganic charge extraction layers. *Science* **350**, 944–948 (2015).
35. Gurudayal, D. Sabba, M. H. Kumar, L. H. Wong, J. Barber, M. Grätzel, N. Mathews, Perovskite–hematite tandem cells for efficient overall solar driven water splitting. *Nano Lett.* **15**, 3833–3839 (2015).
36. J. Luo, J.-H. Im, M. T. Mayer, M. Schreier, M. K. Nazeeruddin, N.-G. Park, S. D. Tilley, H. J. Fan, M. Grätzel, Water photolysis at 12.3% efficiency via perovskite photovoltaics and Earth-abundant catalysts. *Science* **345**, 1593–1596 (2014).
37. C. R. Cox, J. Z. Lee, D. G. Noceraa, T. Buonassisi, Ten-percent solar-to-fuel conversion with nonprecious materials. *Proc. Natl. Acad. Sci. U.S.A.* **111**, 14057–14061 (2014).

38. J. Li, Y. Wang, T. Zhou, H. Zhang, X. Sun, J. Tang, L. Zhang, A. M. Al-Enizi, Z. Yang, G. Zheng, Nanoparticle superlattices as efficient bifunctional electrocatalysts for water splitting. *J. Am. Chem. Soc.* **137**, 14305–14312 (2015).

Acknowledgments

Funding: This work was initiated by the support of the Materials Sciences and Engineering Division, Office of Basic Energy Sciences, U.S. Department of Energy, under contract DEAC02-76-SFO0515. We acknowledge support from the Global Climate Energy Project at Stanford University. This work was also supported by the National Natural Science Foundation of China (21403287) and the Natural Science Foundation of Jiangsu Province, China (BK20140383). We thank M. D. McGehee for his support and helpful discussions. **Author contributions:** Y.Z. and Y.C. designed the experiments and supervised the research. Y.Q. and W.L. performed the experiments. All the other authors contributed to material characterization. All authors discussed the results and commented on the manuscript. **Competing interests:** The authors declare that they have no competing interests. **Data and materials availability:** All data needed to evaluate the conclusions in the paper are present in the paper and/or the Supplementary Materials. Additional data related to this paper may be requested from Y.C. (yicui@stanford.edu) and Y.Z. (ygzhang2012@sinano.ac.cn).

Submitted 4 December 2015
Accepted 26 May 2016
Published 17 June 2016
10.1126/sciadv.1501764

Citation: Y. Qiu, W. Liu, W. Chen, W. Chen, G. Zhou, P.-C. Hsu, R. Zhang, Z. Liang, S. Fan, Y. Zhang, Y. Cui, Efficient solar-driven water splitting by nanocone $BiVO_4$-perovskite tandem cells. *Sci. Adv.* **2**, e1501764 (2016).

ScienceAdvances

Efficient solar-driven water splitting by nanocone BiVO4-perovskite tandem cells

Yongcai QiuWei LiuWei ChenWei ChenGuangmin ZhouPo-Chun HsuRufan ZhangZheng LiangShoushan FanYuegang ZhangYi Cui

Sci. Adv., 2 (6), e1501764. • DOI: 10.1126/sciadv.1501764

Science Advances (ISSN 2375-2548) is published by the American Association for the Advancement of Science. 1200 New York Avenue NW, Washington, DC 20005. The title *Science Advances* is a registered trademark of AAAS.